Molecular Vision 2016; 22:31-39 <http://www.molvis.org/molvis/v22/31>
Received 30 July 2015 | Accepted 14 January 2016 | Published 16 January 2016

Corneal endothelial cells possess an elaborate multipolar shape to maximize the basolateral to apical membrane area

Theresa A. Harrison,[1] Zhiguo He,[2] Kristin Boggs,[3] Gilles Thuret,[2] Hong-Xiang Liu,[3] Dennis M. Defoe[1]

[1]Department of Biomedical Sciences, Quillen College of Medicine, East Tennessee State University, Johnson City, TN; [2]Laboratory "Biology, Engineering, and Imaging of Corneal Graft," BiiGC, Faculty of Medicine, University of Saint Etienne, Saint Etienne, France; [3]Regenerative Bioscience Center, Department of Animal and Dairy Science, College of Agricultural and Environmental Sciences, University of Georgia, Athens, GA

Purpose: The corneal endothelium is widely believed to consist of geometrically regular cells interconnected by junctional complexes. However, while en face visualization of the endothelial apical surface reveals characteristic polygonal borders, the overall form of the component cells has rarely been observed.

Methods: To visualize the shape of individual endothelial cells within the native monolayer, two independent Cre/LoxP-based cell labeling approaches were used. In the first, a *P0-Cre* mouse driver strain was bred to an *R26-tdTomato* reporter line to map neural crest–derived endothelial cells with cytosolic red fluorescent protein. In the second, *HPRT-Cre* induction of small numbers of green and red fluorescent protein–filled cells within a background of unlabeled cells was achieved using a dual-color reporter system, mosaic analysis with double markers (MADM). Selective imaging of the endothelial lateral membranes at different apicobasal levels was accomplished after staining with antibodies to ZO-1 and the neural cell adhesion molecule (NCAM).

Results: When viewed in their entirety in whole-mount preparations, fluorescent protein–filled cells appear star-shaped, extending multiple dendritic processes that radiate outward in the plane of the monolayer. Examination of rare cases where cells expressing different fluorescent proteins lie directly adjacent to one another reveals that these long processes undergo extensive interdigitation. The resulting overlap allows individual cells to extend over a greater area than if the cell boundaries were mutually exclusive. Anti-NCAM staining of these interlocking peripheral cell extensions reveals an elaborate system of lateral membrane folds that, when viewed in optical sections, increase in complexity from the apical to the basal pole. This not only produces a substantial increase in the basolateral, relative to the apical, membrane but also greatly extends the paracellular pathway as a highly convoluted space.

Conclusions: Our analysis indicates that, far from being simple polygonal prisms, endothelial cells possess an elaborate multipolar shape. Their unusual geometry may be essential for the endothelium to carry out its role as the principal regulator of corneal extracellular fluid flux, and thus ultimately of tissue clarity.

The corneal endothelium is a simple layer of epithelial cells strategically positioned at the posterior surface of the cornea. As the anatomic and physiologic boundary between the nutrient-rich aqueous humor and the avascular collagenous stroma, the endothelium plays essential roles in tissue nourishment and transparency by balancing the influx and efflux of extracellular fluids through a pump-leak mechanism [1,2]. As a leaky barrier, the endothelium allows ready access of aqueous humor solutes through the paracellular pathway, while at the same time preventing bulk fluid flow. To limit hydration of the intricate latticework of stromal collagen lamellae, corneal endothelial cells (CECs) use ion and water transport mechanisms to return fluid to the anterior chamber. In this way, the endothelium prevents buildup of extracellular fluids, which is known to cause inhomogeneities in the collagen fibril network and consequent light scattering.

Similar to other transporting epithelia, the corneal endothelium conforms to certain basic principles of tissue structure. Arranged in a closely packed two-dimensional network, CECs are joined together by apically-located circumferential junctional arrays, including adherens junctions that provide tissue integrity and tight junctions that demarcate distinct apical and basolateral membranes and constitute a barrier governing the paracellular pathway. The polarized arrangement of biochemically distinct membranes, in particular, is instrumental in regulating the flux of solutes and fluids via mechanisms involving differentially distributed ion channels and pumps [3,4]. In addition to attributes shared with similar tissues, the endothelium displays other features that are unusual. For example, unlike the cuboidal or columnar cells of most fluid-absorbing or -secreting epithelia, CECs are exceedingly thin, with a smooth apical surface. Such an

Correspondence to: Dennis M. Defoe, Department of Biomedical Sciences, Quillen College of Medicine, East Tennessee State University, Johnson City, TN 37614-0582; Phone: (423) 439-2010; FAX: (423) 439-2017; email:defoe@etsu.edu

attenuated shape is thought to arise from optical requirements that the monolayer minimize light scattering.

During the course of studies on factors regulating corneal endothelium proliferation and differentiation during development, we examined the detailed morphological features of mouse CECs. These studies combined high-resolution immunocytochemical methods with mosaic analysis, in which single labeled cells can be viewed separately from one another in the native endothelium. Our work highlights that individual CECs possess a complex shape that is currently unappreciated. These structural findings may have important consequences for the manner in which these cells operate physiologically to regulate tissue nutrition and extracellular fluid balance.

METHODS

Mouse lines: P0-Cre mice [5] were obtained from K. Yamamura (Kumamoto University School of Medicine). All other strains were purchased from The Jackson Laboratory (Bar Harbor, ME), including *R26-tdTomato* [6] (Stock #007914), *GR-MADM* [7] (Stock #006041), *RG-MADM* [7] (Stock #006067), *HPRT-Cre* [8] (Stock #004302), and C57BL/6J (Stock #000664). Tail snips were taken from transgenic mice on or before 4 weeks of age and frozen prior to processing. Genomic DNA from the tail tissue was extracted with 50 mM sodium hydroxide at 98 °C for 30 min and neutralized with Tris-HCl or, alternatively, processed with the DirectAmp Tissue Kit (Denville Scientific Inc., Metuchen, NJ) which included Preparation (mixture of digestive enzymes) and Extraction (lysis buffer) Solutions. PCR genotyping was conducted to detect *Cre* and *td-Tomato* genes, as well as all *MADM* knock-in alleles. For *P0-Cre* and *td-Tomato*, PCR amplification was carried out with diluted DNA (1:20) under conditions of denaturation at 94 °C for 5 min, followed by annealing at 65 °C for 30 s and extension at 72 °C for 30 s. This cycle was repeated 40 times. In the case of the *HPRT-Cre* gene and *MADM* alleles, DNA was diluted 1:5 prior to thermal steps that included heating to 96 °C for 5 min (initial denaturation), and then 35 cycles of (1) 93 °C for 30 s (denaturation), (2) 55 °C for 30 s (annealing) and (3) 72 °C for 2 min (extension). GoTaq Hot Start Colorless Master Mix (Promega, Madison, WI), containing DNA polymerase, was included in all reactions, along with primer pairs that have been described previously [5-8]. Oligonucleotide products were resolved on 2% agarose gels and visualized after staining with Sybr Gold (Molecular Probes, Eugene, OR). The products and their sizes were as follows: 180 base pairs (bp) long for *P0-Cre*, 196 bp for *td-Tomato*, 220 bp for *HPRT-Cre* and 250 bp for the mutant *MADM* knock-in allele (330 bp for the corresponding wild-type allele). All studies were performed on adult animals (older than 8 weeks) according to protocols approved by the East Tennessee State University (ETSU) University Committee on Animal Care (UCAC), and in accordance with federal guidelines and the ARVO Statement for Use of Animals in Ophthalmic and Vision Research. Strains were maintained free of pathogens in a barrier facility under a 12 h:12 h light-dark cycle.

Generation of conditional reporter and MADM mice: For the conditional reporter studies, the *P0-Cre* strain, which expresses Cre recombinase in post-migratory neural crest cells and their progeny [5], was bred with the *R26-tdTomato* line. In the resulting bitransgenic *P0-Cre;R26-tdTomato* animals, Cre-dependent excision of an upstream stop codon activates expression of the red fluorescent protein (RFP) Tomato in the cytoplasm of neural crest derivatives, including the corneal endothelium. In previous fate mapping studies, Cre recombinase driven by the *P0* promoter has been shown to be expressed in most, but not all, ocular neural crest cells, resulting in areas where CECs are unlabeled [9]. This may be due to incomplete reporter gene activation in *P0-Cre*-positive mice. Alternatively, this could reflect the fact that a subpopulation of endothelial cells is derived from the mesoderm rather than the neural crest [10].

To visualize small numbers of widely distributed fluorescent protein-filled cells, we used mosaic analysis with double markers (MADM). The principles of this technique have been outlined previously [7,11]. Briefly, the site-specific Cre/LoxP recombinase system is used to catalyze recombination between homologous chromosomes carrying transgenes reciprocally chimeric for red (R) and green (G) fluorescent protein. Prior to rearrangement, no functional marker protein is expressed. After Cre-mediated interchromosomal recombination, one or both functional markers are reconstituted within a single cell depending on the types of recombination and segregation [7]. The density of independent marking events can be controlled through the use of an appropriate Cre driver. Because a Cre line specifically targeting the corneal endothelium has not been characterized, we chose to use a ubiquitously expressed transgenic strain [8].

Operationally, mosaic animals were generated using a two-stage breeding regimen. Homozygous *RG* and *HPRT-Cre* mice were first bred to each other. The resulting double-positive *RG/+;HPRT-Cre/+* mice were then crossed to the *GR* line to produce *GR/RG*; *HPRT-Cre/+* mice for MADM analysis [7].

Preparation and processing of whole-mounted corneas: Reporter visualization. Mice were sacrificed by CO2 asphyxiation, and their eyes were isolated and typically fixed in 2%

paraformaldehyde in sodium acetate buffer, pH 6.0 [12]. The corneas surgically dissected from the *P0-Cre;R26-tdTomato* animals were fixed in 4% paraformaldehyde and examined directly following mounting, without antibody-mediated enhancement. In the case of the MADM mice, whole corneas were incubated overnight at 4 °C in combined primary antibodies (chicken anti-green fluorescent protein [GFP]; Aves Labs, Tigard, OR; 1:500, and goat anti-c-Myc; Novus Biologicals, Littleton, CO; 1:200) diluted in Tris-buffered saline (TBS), pH 7.3, with 1.0% bovine serum albumin (BSA) and 0.4% Triton X-100. Anti-c-Myc antibody was preabsorbed with fixed wild-type tissue before use [13]. The following day, the slides were labeled serially with fluorescein isothiocyanate (FITC)–conjugated and Alexa Fluor 555–conjugated secondary antibodies (1:200 and 1:400 dilution, respectively) to enhance visualization of GFP and c-Myc-RFP, respectively. After several buffer rinses, four radial incisions were made in each cornea to produce "petals," and the resulting flatmounts were placed on glass slides with the endothelium facing up and then coverslipped using Vectashield fluorescence mounting medium (Vector Labs, Burlingame, CA) [14].

Immunostaining.: C57BL/6 eyes were fixed as described above, and following dissection, the corneas were subjected to a two-stage labeling procedure. Briefly, after an initial blocking step (normal donkey serum (NDS); 1:10 dilution in TBS-BSA-Triton X-100), the tissues were incubated overnight at 4 °C in rabbit anti-neural cell adhesion molecule (NCAM; EMD Millipore, Temecula, CA; 1:500), then rinsed in buffer, and stained with Alexa Fluor 555–conjugated donkey anti-rabbit immunoglobulin G (IgG; Life Technologies, Carlsbad, CA; 1:400). Before the second stage labeling with the mouse ZO-1 monoclonal antibody (Life Technologies; 1A12; 1:100), the corneas were blocked in NDS, as well as in goat anti-mouse IgG Fab fragments (Jackson ImmunoResearch Laboratories, West Grove, PA; 0.13 mg/ml), to suppress non-specific secondary antibody binding. They were then rinsed in buffer and stained with Alexa Fluor 488–conjugated donkey anti-mouse IgG (Life Technologies) before being flatmounted. Primary antibody incubations took place at 4 °C overnight, while secondary antibodies were applied for 2 h at room temperature.

Microscopy.: Widefield images were acquired using an Olympus BX41 microscope equipped with a 40X (NA=0.75) objective lens and a Micropublisher 3.3 cooled digital camera (QImaging, Surrey, Canada). For confocal microscopy, tissues were viewed in either Leica TCS SP2 or SP8 confocal laser scanning microscopes (Leica, Heidelberg, Germany) equipped with 10X (NA=0.4), 20X (NA=0.7), 63X (NA=1.4), and 100X (NA=1.4) infinity-adjusted objectives. A series of 1-µm- or 0.3-µm-thick optical sections was obtained through the z-axis of individual specimens and used to construct an extended focus image consisting of all optical sections in the data set. For three-dimensional (3D) image reconstruction, series scans were processed using the Leica 3D software module and the resulting images displayed as surface renderings. In some cases, single optical sections were displayed separately. Quantitative data were obtained for ten centrally-located cells, using ImageJ [15] to measure and compare contour lengths at two levels within the endothelium: in the optical section at the apical pole of the cell and in the section at the basal pole near Descemet's membrane where the lateral membrane expansions were largest. Results are expressed as the mean ± standard deviation (SD).

RESULTS

To investigate the overall morphology of endothelial cells, we took advantage of mice engineered to express fluorescent proteins. In Figure 1A, CECs filled with tdTomato appear irregular in outline, showing many peripheral processes that extend outward from the cell bodies into the intercellular space. Occasionally, the occurrence of an area without labeled cells or cell clusters allowed the boundaries of RFP-labeled cells to be viewed more clearly (Figure 1B,C). In these regions, the contrast between the regular geometric shape of the apical cell borders (Figure 1B) and the cell borders at more basal levels (Figure 1C), where red-fluorescing pseudopod-like processes expand from labeled cells into the territory of non-fluorescent cells, is evident.

To visualize single CECs in situ without interference from surrounding cells, we examined mouse corneas using mosaic analysis [7]. Fluorescently labeled cells, scattered throughout the endothelial monolayer (Figure 1D), appear multipolar, with tapered dendritic processes that radiate from cell bodies (Figure 1E–H). Rare examples of labeling where CECs expressing different fluorescent proteins lie directly adjacent to one another demonstrate that these peripheral processes undergo extensive interdigitation (Figure 1E–G).

Optical sections of MADM-labeled corneas were processed using 3D software to render the endothelial cell surfaces (Figure 2). While the reconstructed cells display an impressive range of sizes, shapes, and branching patterns, most exhibit a common set of features. This includes an extended plateau region at the CEC apical pole (c.f., Figure 2B,D,F), from which processes extend initially as ridges with intervening valleys (particularly evident in Figure 2A,C,F) to terminate as finely branched appendages. All surfaces are filled with complex craters and undulations. Basal cell surfaces often present raised star-like impressions as seen

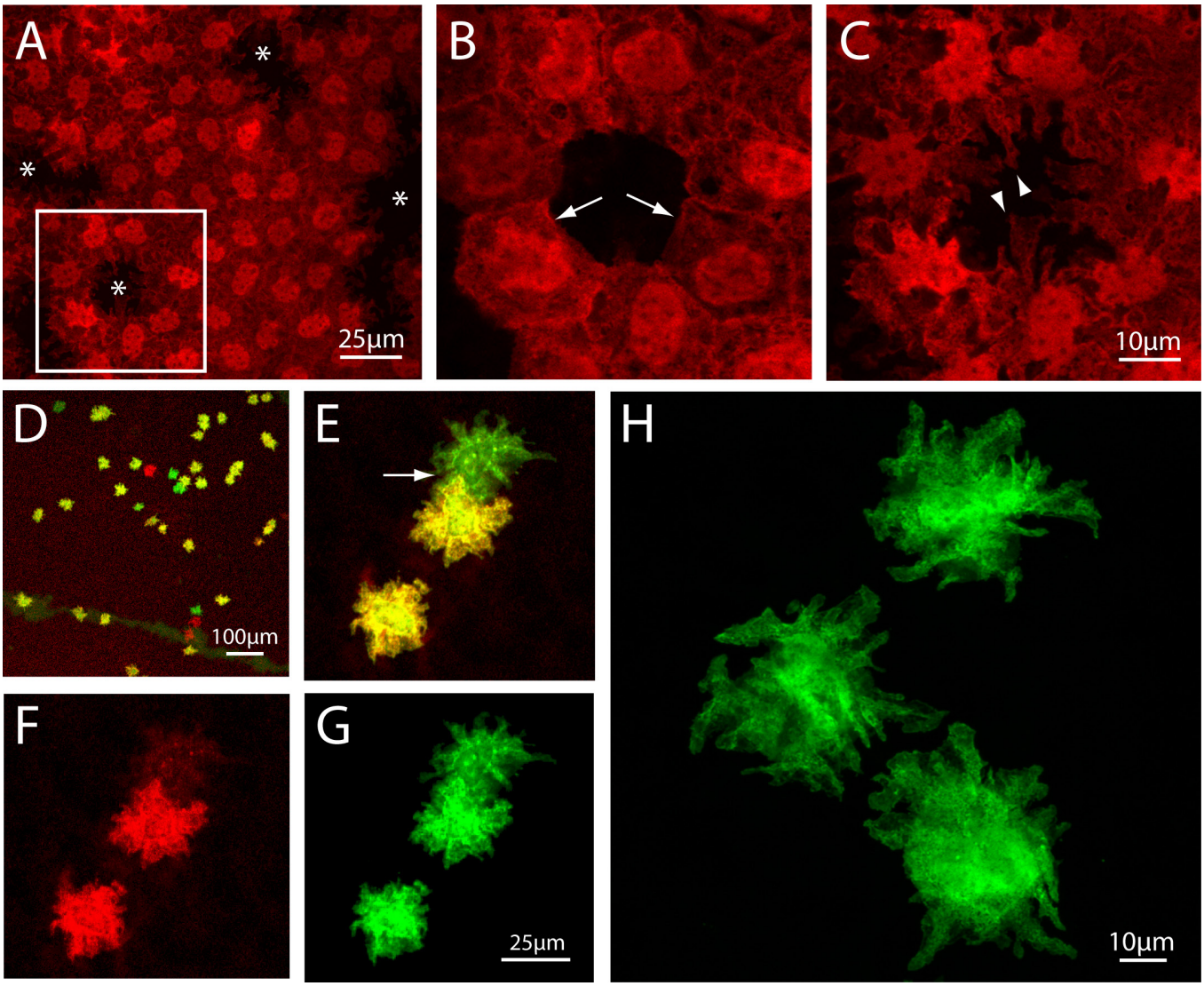

Figure 1. Reporter gene expression in mouse corneal endothelial cells. **A**–**C**: *P0-Cre*-driven expression of *tdTomato*. **A**: In this low-power confocal projection image, the labeled cells exhibit irregular projections that extend in the plane of the monolayer. Asterisks mark areas of non-expressing cells, one of which (indicated by the box) is viewed at higher power in (**B**) and (**C**). **B**: Optical section at 0.3 µm from the apical pole reveals the linear borders of cells where they are connected by junctions (arrows). **C**: At 2.1 µm relative to the apical pole, fluorescent protein expression fills the pseudopod-like processes (arrowheads) that extend into the territory of a non-expressing cell. **D**-**H**: *HPRT-Cre*-mediated mosaic analysis with double markers (MADM) labeling. **D**: Cells marked due to interchromosomal recombination events (see Methods) are scattered among mainly unlabeled endothelial cells in this cornea flatmount viewed at low magnification. This overlay image shows green fluorescent protein (GFP)-expressing (green) cells, c-Myc-red fluorescent protein (RFP)-expressing (red), and cells expressing both fluorescent proteins (yellow). **E**–**G**: A field of view similar to that in **D** is seen at higher power. Where a green cell and a yellow cell occur closely adjacent to one another, their processes can be seen to overlap and interdigitate (arrow in **E**). Images collected in the RFP and GFP channels (**F** and **G**, respectively) compose the overlay image in (**E**). **H**: In this high-magnification image of nearby but non-adjacent MADM-labeled cells, the distinctive star-shaped morphology of corneal endothelial cells, with their branched dendritic processes, can be clearly appreciated. Images **D**–**H** represent projections of all optical sections in the data set.

in the video animation of the reconstructed cell depicted in Figure 2A (Appendix 1), indicating that the cell's interface with Descemet's membrane is not continuous.

In addition to viewing the morphology of whole fluorophore-filled cells, we also examined CECs labeled with probes specific for lateral membrane components. When the apical poles of the cells are imaged by immunolocalization of the tight junction–associated protein ZO-1, individual cells exhibit the familiar polygonal outlines seen previously (Figure 3A). However, an antibody directed against the basolateral marker NCAM [16] reveals a highly elaborate arrangement of membrane ruffles or folds (Figure 3B), as shown recently for the human corneal endothelium [17].

The regional nature of these differences in the cell profile is best appreciated when cells are viewed with confocal microscopy, where optical sectioning in the apicobasal plane discriminates different membrane domains. The series of images in Figure 4 compares the apical portion of intercellular membranes (Figure 4A) with subapical cell contours at increasingly basal levels from the luminal surface to Descemet's membrane (Figure 4B–D). There is a progressive increase in lateral membrane complexity, with projections or undulations of the CEC surface membrane becoming more pronounced as the plane of section approaches the basal cell surface. To quantify this relative expansion of the lateral membranes from apical to basal poles, we traced the membrane contours of the individual cells in the most apical and the most basal optical sections through the cell (Figure 4E,F). This yielded a ratio of basolateral/apical membrane lengths of 3.4±0.4 (2.7–4.0; n=10 cells).

DISCUSSION

Because the physiologic barrier properties of the corneal endothelium are believed to be crucial for its role in maintaining tissue fluid homeostasis and clarity [18,19], most studies have focused on junctional complexes at the posterior face. In addition, perhaps because the corneal endothelium is a relatively flat tissue, only 5 µm thick in humans and 2 µm

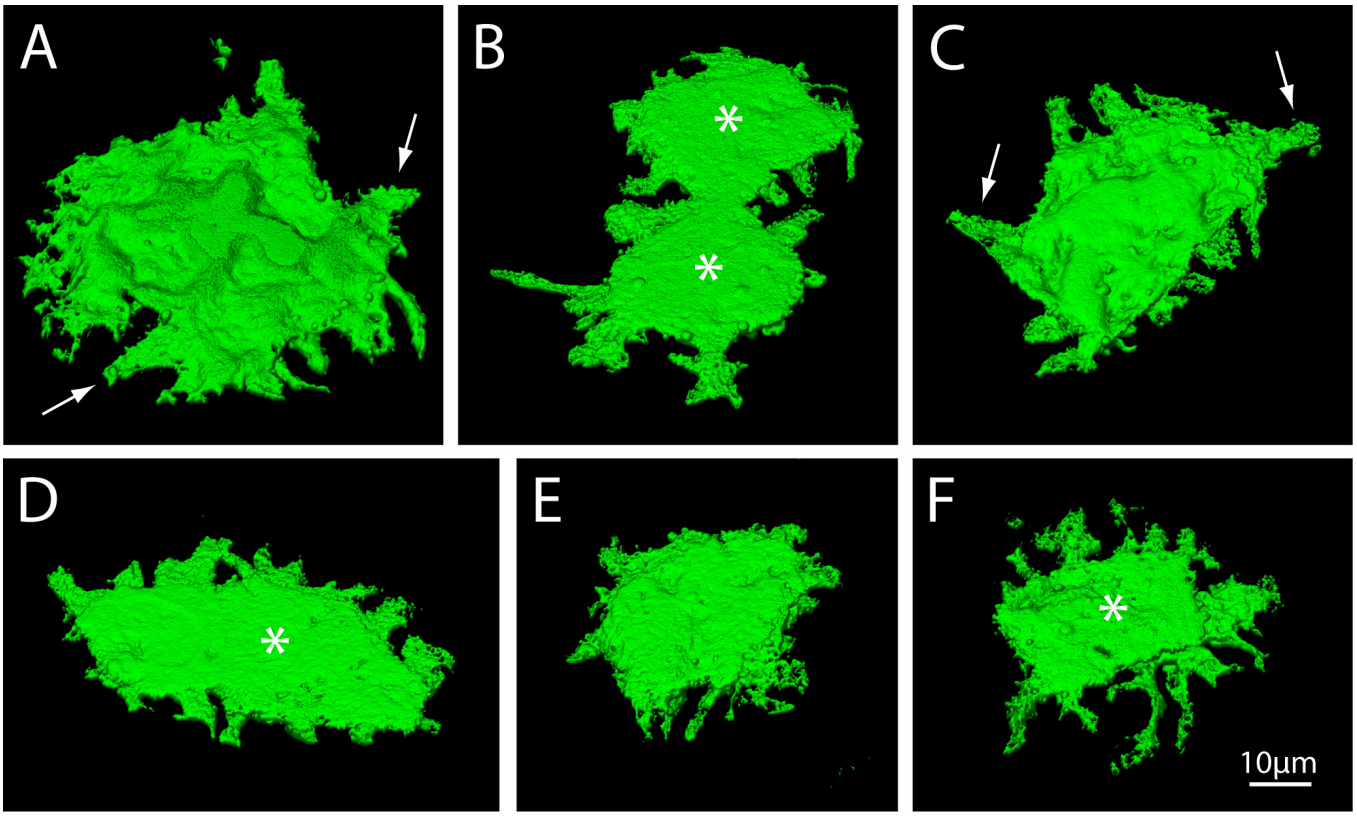

Figure 2. Gallery of endothelial cell surface representations obtained following 3D reconstruction from confocal image stacks. **A**–**F**: Viewed from their anterior surface at 3/4 perspective, mosaic analysis with double markers (MADM)-labeled corneal endothelial cells present flat apical membranes in the form of a plateau region (indicated by asterisks in **B**, **D**, and **F**) that overlaps and partially obscures the dendritic lateral processes. In some cases, the processes can be seen to taper as they extend peripherally and ultimately give rise to smaller branches (arrows in **A** and **C**).

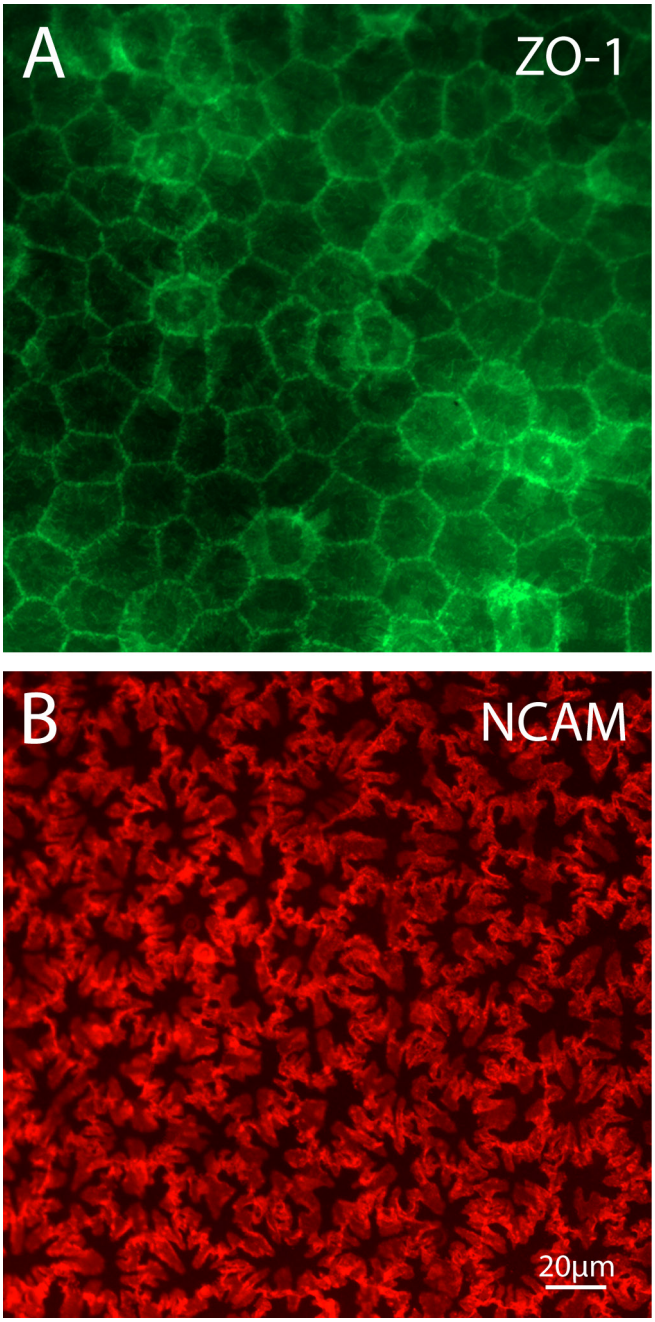

Figure 3. Immunolocalization of corneal endothelial cell lateral membrane markers by widefield fluorescence microscopy. **A**: Reaction of intact tissues with ZO-1 antibody highlights the regular polygonal outlines of cells seen at the level of tight junctions. **B**: Staining for the cell adhesion protein neural cell adhesion molecule (NCAM), however, reveals that much of the interacting surface is in the form of a complex arrangement of membrane folds. When viewing whole cells, this gives the impression of extensive membrane ruffling.

in mice [20,21], its 3D characteristics are easily overlooked when considering its function. Consequently, the apical cell surface, visualized with immunofluorescence or scanning electron microscopy, has often been used as a surrogate for the overall cell shape and as the basis for assessing the general integrity of the tissue. However, when distinct membrane surfaces are revealed using specific probes or individual cells are completely visualized, as in the present study, it becomes clear that the bulk of the CEC surface consists of a complex array of basolateral projections and folds that extend in the plane of the monolayer. The presence of expanded intercellular membranes in a squamous epithelium is unusual and is not accommodated by models of epithelial morphogenesis where the cell height is determined by the amount of membrane targeted to, or removed from, the lateral compartment [22,23]. The existence of such complexity in this tissue is unexpected and suggests an important impact on endothelial function.

Reports indicating that the anterior- and posterior-facing sides of the endothelium may be quite different structurally first appeared more than 30 years ago. Thin section and freeze-fracture electron microscopic studies offered snapshots of limited regions and small samples of the tissue. This resulted in various and somewhat contradictory observations, including a complex jigsaw network of cellular membranes near Descemet's membrane [24], finger-like processes and lateral membrane ruffles [25], and bulbous processes of lateral cell membranes inserting from one cell into its neighbor [26-29]. Based on a sampling of horizontal thin sections taken at different apicobasal levels, Ringvold et al. [30] proposed that the overall form of CECs was similar to that of an octopus, with cell extensions resembling tentacles. It is not clear from these narrowly sampled data if different aspects of the morphology of a single cell population or simply different orientations and/or exemplars of the same morphological features were being described in these studies.

The current study supersedes these reports, providing a complete morphological picture of the cells in this population that unifies the preexisting data and demonstrates that CECs are more complex and extensive in shape than could have been visualized in single thin sections or restricted surface views. Our imaging of entire cells has allowed 3D reconstruction of the overall geometry of CECs for the first time. These data now confirm that the sectioned processes seen previously in electron micrographs are, in fact, dendritic, with complex branching patterns that extend even further laterally than previously proposed. Thus, in our images it becomes

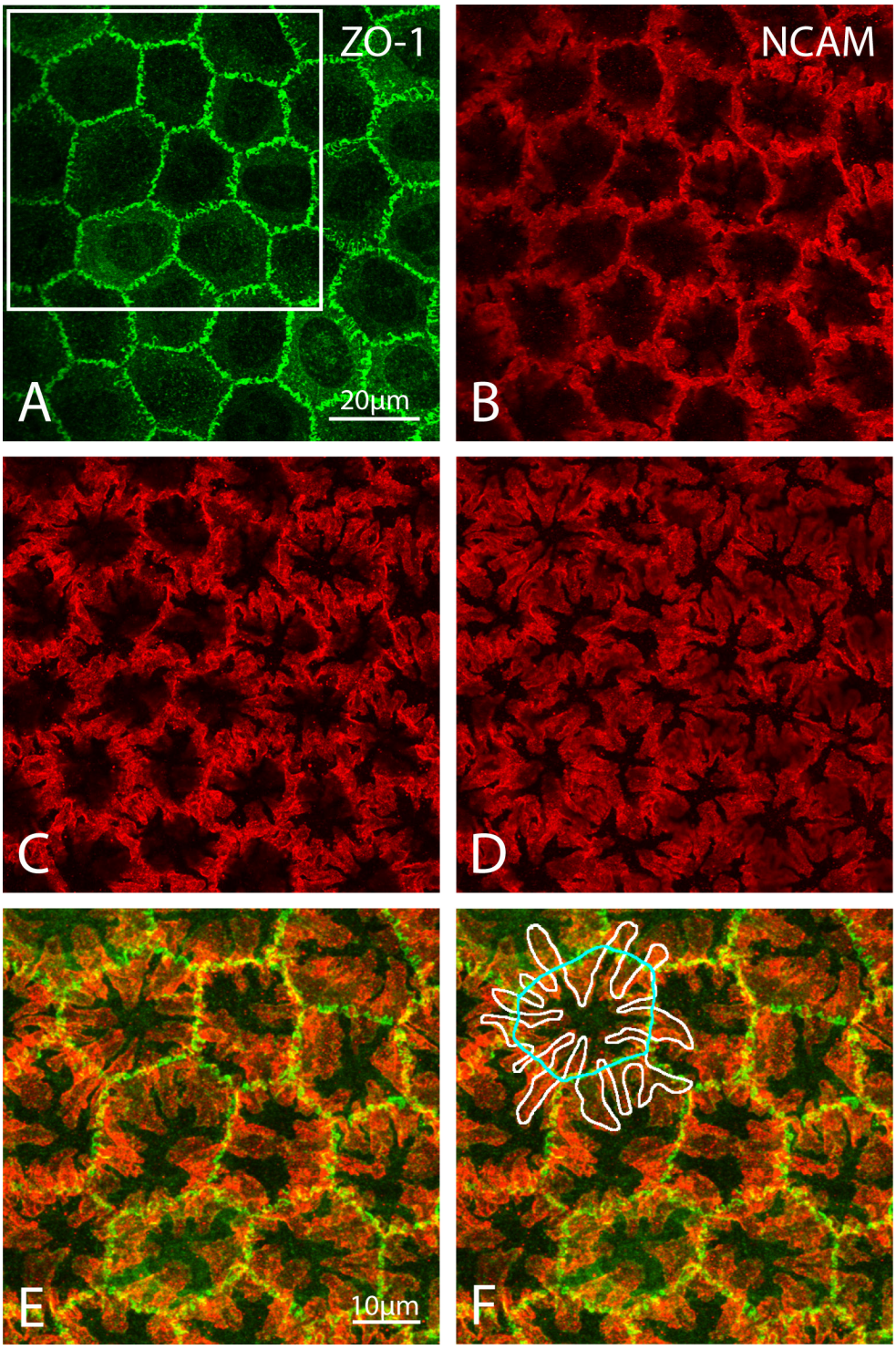

Figure 4. Variation in intercellular boundaries viewed at different apicobasal levels. **A**: ZO-1 antibody delineates the borders of individual cells near the apical corneal endothelial cell (CEC) surface (0.3 µm from the apical pole). **B**–**D**: Imaging of anti-neural cell adhesion molecule (NCAM)-labeled membranes at (**B**) 0.3 µm, (**C**) 1.2 µm, and (**D**) 2.1 µm from the apical pole. In (**B**), the cell boundaries outlined by the NCAM antibody deviate somewhat from those visualized with anti-ZO-1 labeling. A progressive expansion of the CEC lateral membranes is seen as the plane of the optical section passes nearer to the endothelium basal pole (**C**, **D**). **E**: Boxed area in panel (**A**) overlaid with the corresponding region from panel (**D**), shown at higher magnification. Note that the subapical NCAM-containing membranes form expansions that extend centrally and peripherally to the apical (anti-ZO-1-labeled) borders. Using the overlay in (**E**), outlines of a single cell have been drawn at its apical and basal poles (**F**). All images represent single confocal optical sections.

apparent that the diameter of the basolateral aspect of CECs is at least twice that of their apical surfaces. It is also clear that there is substantial heterogeneity among individual cells in the number and complexity of their lateral cell extensions. Neither of these features of CECs could have been addressed or appreciated in previous transmission electron microscopic studies. Viewing cell morphology in its entirety, it becomes clear that the combination of interacting multipolar cells with many intertwined projections leads to the previously described appearance of lateral membrane ruffling when viewed in the electron microscope [25]. The sense of the true endothelial cell shape provided by these new images makes it possible to more accurately envision, and in the future investigate, how individual cells interact in space to create the tissue.

The observed expansion of CEC basolateral membranes may be understood as a structural adaptation to physiologic demands placed on this secretory epithelium, which has the dual requirements of being exceedingly thin while optimizing the amount of "working" membrane. In current models of endothelial fluid transport [2], Na^+/K^+ ATPase activity, in combination with ion transport proteins, is thought to drive anions across the basolateral membrane, with apical membrane channels providing pathways for the coupled movement of ions and water across the cell. The expanded amount of membrane per cell volume provided by the basolateral projections might bolster the function of the endothelial pump, promoting efficient physiologic operation during normal conditions or, perhaps, providing the cell with reserve capacity under conditions of stress. In addition, the complex arrangement of the membranes may have consequences for fluid leak through the paracellular pathway. Using an electron dense tracer to probe extracellular spaces, Kreutziger [28] emphasized the tortuosity of interdigitating lateral cell boundaries, where intercellular contacts containing gap junctions encompass extensive regions, limiting the width of the interspace. Thus, the elaborate foldings of cell membranes may act as geometric factors restricting the extracellular passage of molecules and, consequently, the operation of the intercellular space as a potential barrier.

The extent to which the overall health of the corneal endothelium depends upon, or is reflected in, the maintenance of specific geometric characteristics, requires further examination. In clinical applications, morphological indicators are used to evaluate tissue potential for success in corneal transplant, but the correlation between the two has not always proved reliable [31]. Such indicators are typically limited to those provided by non-invasive assessment of the posterior (or apical, in the present study) tissue surface [32]. In this regard, our results suggest that visualization of the lateral boundaries of cells would contribute more information about tissue architecture that may be relevant to the underlying physiologic conditions. It remains to be determined if disruption of the intricate interrelationships between CECs in the basolateral domain occurs earlier and/or more readily, and with more or less functional consequence, than disruption of the tight junction barrier. Thus, it could be useful in the future to collect such data in a clinical context.

APPENDIX 1. VIDEO ANIMATION OF 3D RECONSTRUCTED MADM-LABELED CORNEAL ENDOTHELIAL CELL FROM FIGURE 2A.

To access the data, click or select the words "Appendix 1."

ACKNOWLEDGMENTS

This research was supported by the National Institutes of Health (R15EY17997 to DMD and R01DC012308 to HXL), the ETSU Research Development Committee (to DMD), and by ANR Tecsan 2012, Project Corimmo 3D and Etablissement Français du Sang AP Recherche 2011 (to GT). It was also supported by NIH grant C06RR0306551. We are grateful to Dr. Kenichi Yamamura for providing the *P0-Cre* mice.

REFERENCES

1. Mergler S, Pleyer U. The human corneal endothelium: new insights into electrophysiology and ion channels. Prog Retin Eye Res 2007; 26:359-78. [PMID: 17446115].
2. Bonanno JA. Molecular mechanisms underlying the corneal endothelial pump. Exp Eye Res 2012; 95:2-7. [PMID: 21693119].
3. Bryant DM, Mostov KE. From cells to organs: building polarized tissue. Nat Rev Mol Cell Biol 2008; 9:887-901. [PMID: 18946477].
4. Spring KR. Epithelial fluid transport – a century of investigation. News Physiol Sci 1999; 14:92-8. [PMID: 11390829].
5. Yamauchi Y, Abe K, Mantani A, Hitoshi Y, Suzuki M, Osuzu F, Kuratani S, Yamamura K. A novel transgenic technique that allows specific marking of the neural crest cell lineage in mice. Dev Biol 1999; 212:191-203. [PMID: 10419695].
6. Madisen L, Zwingman TA, Sunkin SM, Oh SW, Zariwala HA, Gu H, Ng LL, Palmiter RD, Hawrylycz MJ, Jones AR, Lein ES, Zeng H. A robust and high throughput Cre reporting and characterization system for the whole mouse brain. Nat Neurosci 2010; 13:133-40. [PMID: 20023653].
7. Zong H, Espinosa JS, Su HH, Muzumdar MD, Luo L. Mosaic analysis with double markers in mice. Cell 2005; 121:479-92. [PMID: 15882628].

8. Tang SH, Silva FJ, Tsark WM, Mann JRA. Cre/loxP-deleter transgenic line in mouse strain 129S1/SvImJ. Genesis 2002; 32:199-202. [PMID: 11892008].

9. Iwao K, Inatani M, Okinami S. Fate mapping of neural crest cells during eye development using a *protein 0* promoter-driven transgenic technique. Graefes Arch Clin Exp Ophthalmol 2008; 246:1117-22. [PMID: 18458932].

10. Gage PJ, Rhoades W, Prucka SK, Hjalt T. Fate maps of neural crest and mesoderm in the mammalian eye. Invest Ophthalmol Vis Sci 2005; 46:4200-8. [PMID: 16249499].

11. Henner A, Ventura PB, Jiang Y, Zong H. MADM-ML, a mouse genetic system with increased clonal efficiency. PLoS One 2013; 8:e77672-[PMID: 24143253].

12. Lorincz A, Nusser Z. Molecular identity of dendritic voltage-gated sodium channels. Science 2010; 328:906-9. [PMID: 20466935].

13. Espinosa JS, Luo L. Timing neurogenesis and differentiation: insight from quantitative clonal analyses of cerebellar granule cells. J Neurosci 2008; 28:2301-12. [PMID: 18322077].

14. Defoe DM, Adams LBS, Sun J, Wisecarver SN, Levine EM. Defects in retinal pigment epithelium cell proliferation and retinal attachment in mutant mice with $p27^{Kip1}$ gene ablation. Mol Vis 2007; 13:273-86. [PMID: 17356514].

15. Schneider CA, Rasband WS, Eliceiri KW. NIH Image to ImageJ: 25 years of image analysis. Nat Methods 2012; 9:671-5. [PMID: 22930834].

16. Foets BJ, van den Oord JJ, Volpes R, Missotten L. In situ immunohistochemical analysis of cell adhesion molecules on human corneal endothelial cells. Br J Ophthalmol 1992; 76:205-9. PMID: 1382576[PMID: 1382576].

17. Forest F, Thuret G, DuMollard JM, Peoc'h M, Perrache C, He Z. Optimization of immunostaining on flat mounted human corneas. Mol Vis 2015; 21; 1345 1356.

18. Stocker FW. The endothelium of the cornea and its clinical implications. Trans Am Ophthalmol Soc 1953; 51:669-786. [PMID: 13216798].

19. Edelhauser HF. The balance between corneal transparency and edema: the Proctor Lecture. Invest Ophthalmol Vis Sci 2006; 47:1754-67. [PMID: 16638979].

20. Waring GO 3rd, Bourne WM, Edelhauser HF, Kenyon KR. The corneal endothelium: normal and pathologic structure and function. Ophthalmology 1982; 89:531-90. [PMID: 7122038].

21. Henriksson JT, McDermott AM, Bergmanson JPG. Dimensions and morphology of the cornea in three strains of mice. Invest Ophthalmol Vis Sci 2009; 50:3648-54. [PMID: 19264894].

22. Cai L, Mostov KE. Cell height: Tao rising. J Cell Biol 2012; 199:1023-4. [PMID: 23266952].

23. Gomez JM, Wang Y, Riechmann V. Tao controls epithelial morphogenesis by promoting Fasciclin 2 endocytosis. J Cell Biol 2012; 199:1131-43. [PMID: 23266957].

24. Hirsch M, Renard G, Faure J-P, Pouliquen Y. Study of the ultrastructure of the rabbit corneal endothelium by the freeze-fracture technique: apical and lateral junctions. Exp Eye Res 1977; 25:277-88. [PMID: 590370].

25. Sherrard ES, Ng YL. The other side of the corneal endothelium. Cornea 1990; 9:48-54. [PMID: 2297995].

26. Iwamoto T, Smelser GK. Electron microscopy of the human corneal endothelium with reference to transport mechanisms. Invest Ophthalmol 1965; 4:270-84. [PMID: 14326614].

27. Kaye GI. Studies on the cornea. III. The fine structure of the frog cornea and the uptake of colloidal particles by the cornea in vivo. J Cell Biol 1962; 15:241-58. [PMID: 14042126].

28. Kreutziger GO. Lateral membrane morphology and gap junction structure in rabbit corneal endothelium. Exp Eye Res 1976; 23:285-93. [PMID: 976372].

29. Ottersen OP, Vegge T. Ultrastructure and distribution of intercellular junctions in corneal endothelium. Acta Ophthalmol 1977; 55:69-78. [PMID: 402786].

30. Ringvold A, Davanger M, Olsen EG. On the spatial organization of the cornea endothelium. Acta Ophthalmol 1984; 62:911-8. [PMID: 6524316].

31. Bourne WM. Biology of the corneal endothelium in health and disease. Eye (Lond) 2003; 17:912-8. [PMID: 14631396].

32. Doughty MJ. Toward a quantitative analysis of corneal endothelial cell morphology: a review of techniques and their application. Optom Vis Sci 1989; 66:626-42. [PMID: 2677883].

Articles are provided courtesy of Emory University and the Zhongshan Ophthalmic Center, Sun Yat-sen University, P.R. China. The print version of this article was created on 16 January 2016. This reflects all typographical corrections and errata to the article through that date. Details of any changes may be found in the online version of the article.